# CFD MULTIPHASE MODELING OF BLOOD CELLS SEGREGATION IN FLOW THROUGH MICROTUBES

**Rakhim Supiyev,** B. Eng and Technology

**Submitted in fulfilment of the requirements**

**for the degree of Masters of Science**

**in Mechanical Engineering**


**School of Engineering**

**Department of Mechanical Engineering**

**Nazarbayev University**

53 Kabanbay Batyr Avenue,

Astana, Kazakhstan, 010000

**Supervisor:** Luis R. Rojas-Solórzano

**Co-supervisor**: Konstantinos Kostas

**December 2017**

DECLARATION

I hereby, declare that this manuscript, entitled “CFD Multiphase Modeling of Blood Cells Segregation in Flow through Microtubes”, is the result of my own work except for quotations and citations which have been duly acknowledged.

I also declare that, to the best of my knowledge and belief, it has not been previously or concurrently submitted, in whole or in part, for any other degree or diploma at Nazarbayev University or any other national or international institution.

_ _ _ _ _ _ _ _ _ _ _ _ _ _ _ _ _ _ _

Name:

Date:

# Abstract

Cardiovascular diseases, commonly referred as Heart Diseases, involve heart and blood vessels associated to the cardiovascular system. So called blood wetted medical devices are widely used in treatment of heart diseases as they help to provide better blood flow to patients. However, when blood is flowing through medical devices, it can be damaged due to lack of compatibility with surrounding non-biological walls of pipes, connectors and containers, thermal and osmotic effects, or most prominently due to excessive shear stresses on blood cells by medical devices. Though laboratory tests are vital for design improvements, they have proven to be costly, time intensive and ethically controversial. On the other hand, Computational Fluid Dynamics is a promising and inexpensive tool for simulating blood flow. The aim of this project is to improve and validate existing numerical model of blood cells segregation in flow through microtube. An improved numerical model of blood cells segregation is of interest for further evaluation of blood damage for design purposes of medical devices. The proposed model is based on Granular Kinetic Theory and represents a continuation of previous work by Mendygarin et al. [4] by sensitive analysis of red blood cells Sauter diameter according to local flow conditions.

# Acknowledgements

Firstly, I will like to express the deepest appreciation to my supervisor Luis R. Rojas-Solórzano and co-supervisor Konstantinos Kostas. I would like to express my uttermost gratitude for all the hours of discussion they have offered me. Without their guidance and persistent help this thesis would not have been possible. It has been their supervision and direction, stimulating my suggestions and encouragement throughout the duration of my studies which has allowed me to successfully complete the Master's program.

Secondly, I will like to show my indebtedness to the School of Engineering staff at Nazarbayev University whose efforts a lot of time go unnoticed.

Finally, I would like to thank my parents upon whose shoulders I stand.

# Table of Contents

# List of Abbreviation & Symbols

| | |
|---|---|
| $\rho_r$ | Density of the RBC |
| $\rho_s$ | Density of the PLT |
| $\rho_f$ | Density of the plasma |
| $c_d$ | Drag coefficient |
| $\varepsilon_f$ | Volume fraction of plasma |
| $\varepsilon_r$ | Volume fraction of RBC |
| $\varepsilon_s$ | Volume fraction of PLT |
| $\vec{v}_f$ | Velocity of plasma vector |
| $\vec{v}_r$ | Velocity of RBC vector |
| $\vec{v}_s$ | Velocity of PLT vector |
| $\vec{g}$ | Gravitational acceleration |
| $\nabla P$ | Pressure gradient |
| $\nabla P_f$ | Plasma pressure gradient |
| $\nabla P_r$ | RBC pressure gradient |
| $\nabla P_s$ | PLT pressure gradient |
| $\vec{\vec{\tau}}_f$ | Plasma stress tensor |
| $\vec{\vec{\tau}}_r$ | RBC stress tensor |
| $\vec{\vec{\tau}}_s$ | PLT stress tensor |
| $\beta$ | Drag exchange coefficient |
| $\theta$ | Granular temperature |
| $\vec{\vec{I}}$ | Unit tensor |
| $k$ | Granular conductivity |
| $k_r$ | RBC extinction coefficient of the absorbing medium |
| $k_s$ | PLT extinction coefficient of the absorbing medium |
| $\gamma$ | Energy dissipation |
| $y_e$ | Equilibrium position |

# List of Tables

# List of Figures

# List of Publications

Mendygarin Y., Kussaiyn N., Luis R. Rojas-Solórzano, Zhussupbekov M., Supiyev R., 2017, "Eulerian-Eulerian Multiphase Modeling of Blood Cells Segregation in Flow through Microtubes," ASME IMECE 2017 Proceedings, in press

Supiyev R., Luis R. Rojas-Solórzano, Mubita T. M., Zhussupbekov M., Zhanshayeva L., 2018, "CFD Multiphase Modeling of Blood Cells Segregation in Flow through Microtubes," AIDIC IBIC 2018, accepted abstract, full paper in progress

# Chapter 1 – Introduction

## 1.1 General

Cardiovascular diseases (CVD) are the leading cause of deaths worldwide. Approximately 17.5 million people died from CVD in 2012. That number represents 31% of all deaths [1]. By 2030, estimated number of deaths due to CVD will reach to more than 23.6 million. Surgical treatment of cardiovascular diseases requires the use of devices that will be in direct contact with blood flow. However, blood might be damaged due to biological incompatibility with materials used in the interface of these devices or due to exposure to high shear stresses, above a threshold value, for a prolonged period of time. These stress levels may lead to release of hemoglobin from red blood cells (RBCs) to plasma in process called hemolysis. Additionally, the exposure to considerable shear stress on platelets (PLTs) during significant period of time may trigger the emergence of thrombosis [2]. Therefore, exposition of blood cells to shear stresses requires special consideration for a proper and careful design of blood wetted medical devices (BWMD) in order to avoid blood trauma. Nonetheless, vital for design purposes, in-vitro experiments can be expensive and raise ethical issues. Therefore, simulation of blood flow using Computational Fluid Dynamics (CFD) has risen as a promising and inexpensive tool. Nevertheless, current state-of-the-art CFD models are still far from being reliable and accurate for design purposes [3]. The

attempt of this study is to improve and validate previous model by Mendygarin et al. [4] by optimization analysis of RBCs' Sauter diameter with dependence on local flow field conditions. Thus, the main hypothesis of this investigation is that the main limitation of the model proposed by Mendygarin et al. lies on their consideration of every RBC as a spherical-like rigid body. As experienced in a simple shear flow, RBCs reveal different geometries and dynamics. An inexpensive CFD model prepared with state-of-the-art software ANSYS FLUENT could not catch these shape irregularities of RBCs, unless computationally expensive direct numerical simulation is performed, which is still out of bounds for engineering applications. Hence, development of a model with improved prediction of blood cells segregation, yet computationally affordable, will allow proposing an adequate blood cell damage model (e.g. hemolysis or thrombosis) to be used in CAE optimization of BWMD in the future.

## 1.2 Aim & Objectives

The aim of this work is to improve an existing numerical model for blood cells segregation in a microtube, which ultimately would provide a solid base for accurate prediction of blood damage. The specific objective of this research is to develop and validate a model for prediction of blood cell segregation, based on the incorporation of an improved model of RBCs Sauter diameter that considers biological deformations observed in the surface of these cells when subject to different blood flow regimes.

## 1.3 Methodologies and techniques

In the model developed in this MSc thesis, blood is considered as a multiphase substance composed of plasma, RBCs and PLTs. Simulations based on finite volume method and departing from an existing Eulerian-Eulerian multiphase model with partial success, assessed in a previous work, serve as base case model which is enhanced by considering cell-to-cell interactions through the introduction of the Granular Kinetic Theory (GKT) for treatment of the disperse phases (RBC and PLT). GKT proved to be a good model for prediction of particle concentration and pressure drop by considering kinetic, collisional and frictional effects of the solid phases. The key point of this study to take into account shape irregularities of RBCs. It was expected that consideration of RBCs shape evolution would help to develop a more realistic flow of blood cells and, consequently, improve the existing model of blood cells segregation in microtubes.

## 1.4 Thesis structure

This thesis consists of separate sections to present: (a) literature review on experiments and simulations of blood cells spatial distribution in flow through pipes; (b) deformation of RBCs; (c) methodology and implementation of the proposed model; and ends up with (d) results and concluding remarks.

# Chapter 2 – Literature Review

## 2.1 Blood flow behavior. Fahraeus-Lindquist effect

It has been recognized that in blood flow, the interactions between RBCs with each other and with PLTs lead to a special distribution of cells in blood vessels. Furthermore, RBCs tend to accumulate at the center of blood vessels, where they displace PLTs and force them to move toward the walls of vessels [5]. This behavior of blood cells in flow is denominated Fahraeus-Lindqvist (F-L) effect.

## 2.2 Models of blood cells spatial distribution in flow through tubes

### 2.2.1 Experiments by Yeh et al. [6]

The F-L effect is reproduced in experiments by Yeh et al. [6]. Authors conducted experiments using a capillary tube with 217 μm in diameter (which is equivalent to 35 times mean Sauter diameters of the RBC), 40% hematocrit of RBCs and 2.5 μm latex particles as PLTs. Figure 2.1 represents PLTs relative concentration in capillary tube in experiments by Yeh et al.

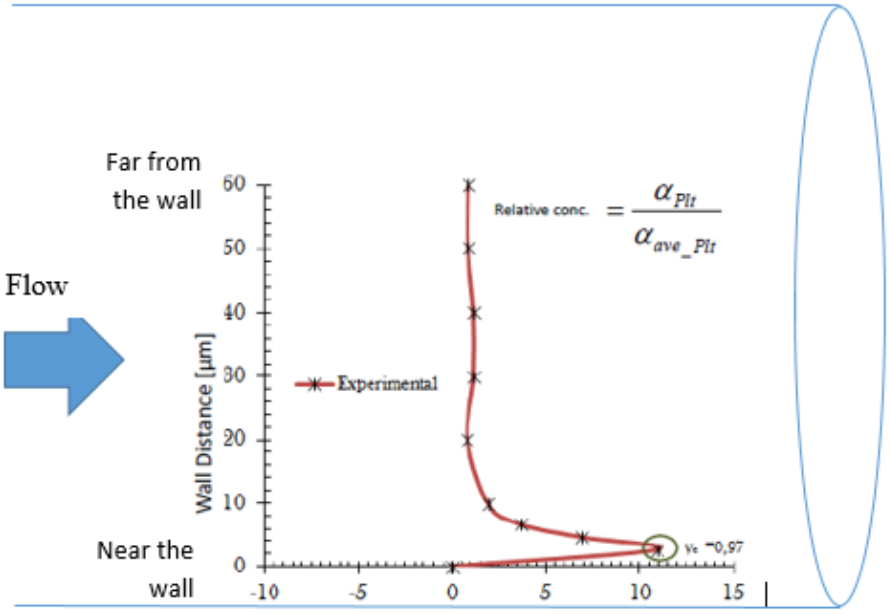


***Figure 2.1: PLTs-like relative concentration (source: Yeh et al. [6])***

### 2.2.2 Multiphase model by Mubita et al. [7]

The multiphase model by Mubita et al. [7] is oriented to reproduce the experimental work of blood flow in capillary tube by Yeh at al. [6]. In Mubita et al's model, blood cells (taken as the fluid dispersed phase) interact strongly with plasma (continuum phase). The model improved predecessor studies of blood cells segregation. Authors acknowledged, that although the model catches the segregation of PLTs, it under-predicts the peak PLTs concentration near the wall.

### 2.2.3 Blood segregation model by Mendygarin et al. [4]

The multiphase model by Mendygarin [4] with incorporated GKT for dispersed phases demonstrated an improvement of around 7% comparing to the model by Mubita et al. [7] in the prediction of the peak PLTs concentration, by prescribing a tuned cell-plasma drag coefficient and cells Sauter diameter.

Mendygarin et al. in their model considered cell-to-cell interaction, while the model of Mubita et al. takes into account only cell-to-plasma interaction.

### 2.2.4 Other numerical models to explain Fahraeus-Lindquist effect

Gidaspow and Huang [8] conducted numerical simulations based on GKT theory to predict blood cells spatial distribution validated through reproduction of F-L effect. According to GKT, granular temperature is the driving force for migration of RBCs toward the center of the tube due to inelastic collisions among RBCs. Authors concluded that their computed model of hematocrit distribution agrees with experimental data.

Similar research on migration of RBCs from the walls toward the center of narrow tubes was conducted by Tandon et al. [9]. Authors used two different approaches: GKT and two-fluid based suspension rheology. Simulations results for both models agree with experimental measurements, although the model based on GKT predicts hematocrit concentration near the wall better than the suspension rheology model because it takes into account the inelasticity of the walls.

Although the models of Gidaspow and Huang [8] and Tandon et al. [9] estimate RBC concentration acceptably well, Mubita et al. [7] mentioned that authors did not take into account the presence of PLTs.

## 2.3 Studies on RBC deformation

As mentioned before, the model by Mendygarin et al. [7] considers the RBC as a spherical rigid body and it is definitively a rough approximation. The hypothesis of this study is that the consideration of shape deformation of RBCs will improve prediction of blood cells segregation within the flow in a microtube.

### 2.3.1 RBC membrane structure. The work of Sigüenza [10] using optical tweezers

Sigüenza [10] in his study addresses issues of modeling of complex microstructure of the RBC membrane interacting with outer liquid (plasma). The RBC has a discocyte shape with the average dimensions measured by Evans and Fung [11] represented in Figure 2.2.

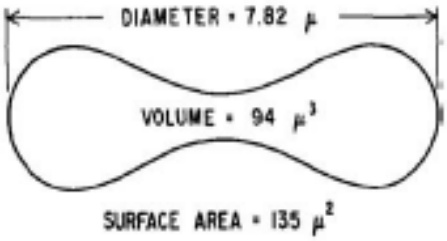


***Figure 2.2: Average dimensions of RBC (source: Evans and Fung [11])***

The RBC consists of a membrane, which encloses an internal fluid. RBCs are subjected to deformation when flowing in vessels mainly due to the following reasons: the deflated structure of a geometry, which is caused by a greater membrane surface area than the surface of a sphere with the same volume; the specific composite structure of the membrane of RBC. As it can be seen from

Figure 2.3, the membrane of the RBC consists of a lipid bilayer and the cytoskeleton which is connected to a lipid bilayer with transmembrane proteins.

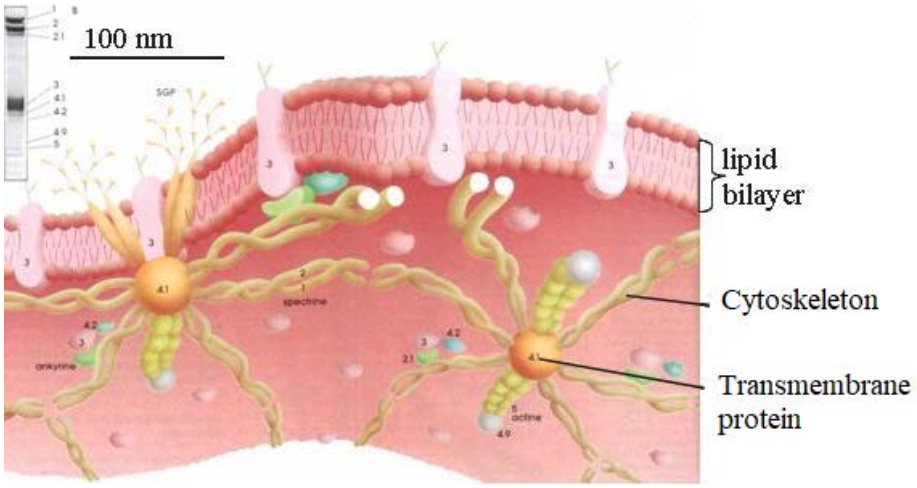


***Figure 2.3: RBC membrane structure (source: http://www.msc.univ-paris-diderot.fr/~frgallet/Research_Activities/Research.html)***

A lipid bilayer is responsible for resisting to bending deformation and area-dilation. The cytoskeleton is responsible for resisting to shear deformation and area-dilation as well.

In order to accurately predict RBCs deformation with dependence on wide range of local flow conditions, Mohandas and Evans [12] developed an experiment using optical tweezers, which allowed them to investigate a large range of deformations of RBCs. Figure 2.4 describes the experiment with the optical tweezers.

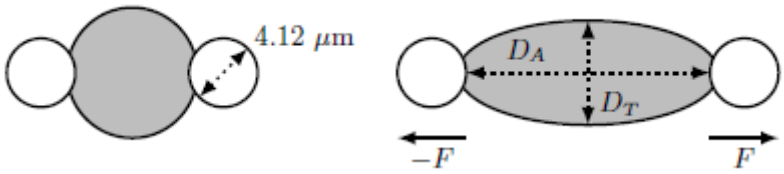


***Figure 2.4: The optical tweezers experiment (source: Mills et al. [13])***

Two microbeads (each 4.2 μm) are attached at the opposite regions. Force is applied at two microbeads in order to stretch the cell. The deformed shape can be calculated using the following expression by Mohandas [12]:

$$z = \pm 0.5 R_0 \left[1 - \frac{x^2 + y^2}{R_0^2}\right]\left[A + B\frac{x^2 + y^2}{R_0^2} + C\left(\frac{x^2 + y^2}{R_0^2}\right)^2\right]$$

where $R_0 = 3.91\mu m$ is the average radius of RBC.

Figure 2.5 represents the shapes of deformed RBC for different applied forces. When increasing the force, the shape of RBC starts to elongate and becomes elongated. The same shapes of RBC after deformation were obtained by Mills et al. [13].


***Figure 2.5: A half of the RBC. Deformation of the RBC over the range of forces (source: Sigüenza [10])***

The model for calculation of deformation of RBC's membrane proposed by those authors agrees fairly well with experimental measurements by optical tweezers.

### 2.3.2 Experiments using optical tweezers by Dao et al. [14]

Another research using optical tweezers was conducted by Dao et al. [14]. Authors obtained similar to described above deformations of shapes by applying different magnitude of forces. Dao et al. [14] concluded that the results of their work agree with a wealth of experimental information in literature on deformation of RBCs, e.g. Evans and Skalak [15] and Fung [16].

# Chapter 3 – Modeling Methodology

## 3.1 Effect of velocity of the flow on the RBC's shape

The proposed numerical simulations of blood flow in this investigation are based on an Eulerian-Eulerian multiphase model including the GKT for treatment of dispersed phases. The model is oriented to reproduce the experiments of blood flow by Yeh et al. [6] validated through reproduction of F-L effect. Moreover, the model developed in this MSc thesis aims to improve previous models of blood cells segregation by prescription of sensible RBC diameter across the flow, with dependence on local flow conditions. Therefore, the developed model, based on experiments, required the investigation of deformation of RBCs with dependence on different conditions.

Let's firstly introduce experimental work developed by other authors on RBC deformation due to flow field conditions. Among them, Secomb [17] studied transition of RBCs shapes under variation of flow velocity. Figure 3.1 presents the results of the experiments: as velocity increases, the RBC elongates in the capillary tube of fixed diameter 6 μm.

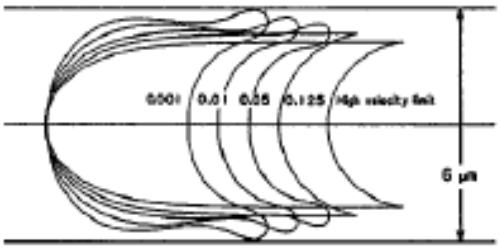


***Figure 3.1: Transition of the shape of RBC with increasing of flow velocity (source: Secomb [17])***

Another experiments by Faivre [18], on which this model is oriented, uses microscope, high-speed camera with the frame rate of up to 10,000 frames/second and image analysis software, as: National Institute of Health Image J 1.32j and MATLAB in order to determine cells velocity, volume, dimension, orientation and other parameters.

As it is widely known, RBCs can reveal different movements under shear flow (see Figure 3.2).

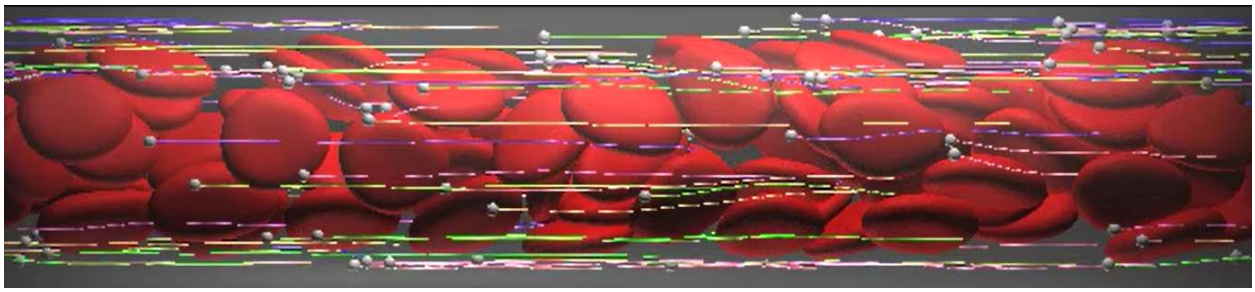

***Figure 3.2: The flow of RBCs for hematocrit $Hct = 0.2$, $Ca = 0.2$ in the vessel with diameter $D = 22\mu m$ (image courtesy of Takeshi and Imai [19])***

It is generally accepted, that the two possible movements of RBCs are: unstable tumbling motion (when RBC moves like a flipping coin) and tank-treading motion (when RBC rotates around itself). Faivre [18] proposed a vertical “swinging”

motion (when the RBC moves in vertical position with small oscillations), claiming that this kind of motion better shows the existence of the RBC membrane's shape memory and help to determine the elastic shear modulus. Figure 3.3 represents a vertical flow of RBCs in a micro-vessel [19].

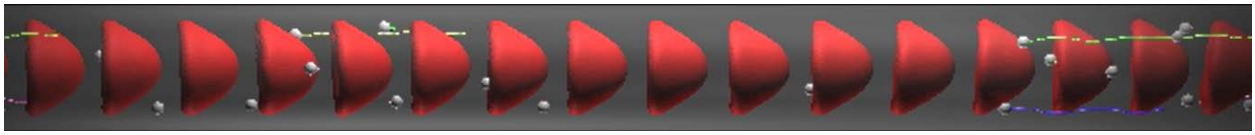

***Figure 3.3: A vertical "swinging" flow of RBCs for hematocrit $Hct = 0.2$, $Ca = 0.2$ in the vessel with diameter $D = 10\mu m$ (image courtesy of Takeshi and Imai [19])***

The shape of RBCs represented in Figure 3.3 reveals axisymmetric parachute-like form. If velocity keeps increasing, RBCs will take form of a non-axisymmetric slipper-like shape. As it can be seen from Figure 3.4, the shape of RBC starts to develop a "tail", which becomes sharper and thinner as velocity of flow increases (experiments by Faivre [18]). Similar shapes are observed in experiments [20, 21].

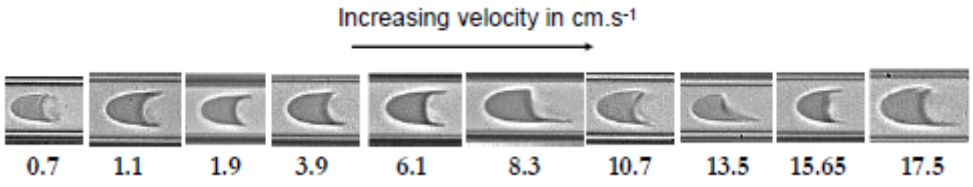


***Figure 3.4: Evolution of the RBC from parachute-like toward slipper-like shape with increasing of velocity (source: Faivre [18])***

The results agree with the prediction of RBCs shapes by Pozrikidis [22]. The effect of viscosity of outer liquid and capillary diameter on the shape of RBC also

were studied by Faivre [18]. However, these effects are not included in this study, since viscosity of plasma and diameter of the microtube are fixed in the proposed model of this MSc thesis. To summarize the study, Faivre developed a phase diagram of the RBC shape transitions, which is represented in Figure 3.5. X-axis on the diagram is a size of the RBC (*a/R*, non-dimensional) and Y-axis is an external stress ($\eta_{out}V$, $Pa \times s$), where *a* is a typical size of a RBC, *R* is the radius of the capillary, $\eta_{out}$ is a viscosity of the outer fluid (plasma) and *R* is velocity of the flow. The three regions can be defined out of the diagram: the top left region – non-axisymmetric (slipper-like) shape and non-centered (the center of the RBC is offset compared to the center of the tube), the top right region – non-axisymmetric shape and centered, the bottom region – axisymmetric (parachute-like) shape. Transition from axisymmetric parachute-like to non-axisymmetric slipper-like shape happens around $\eta_{out}V = 0.001$

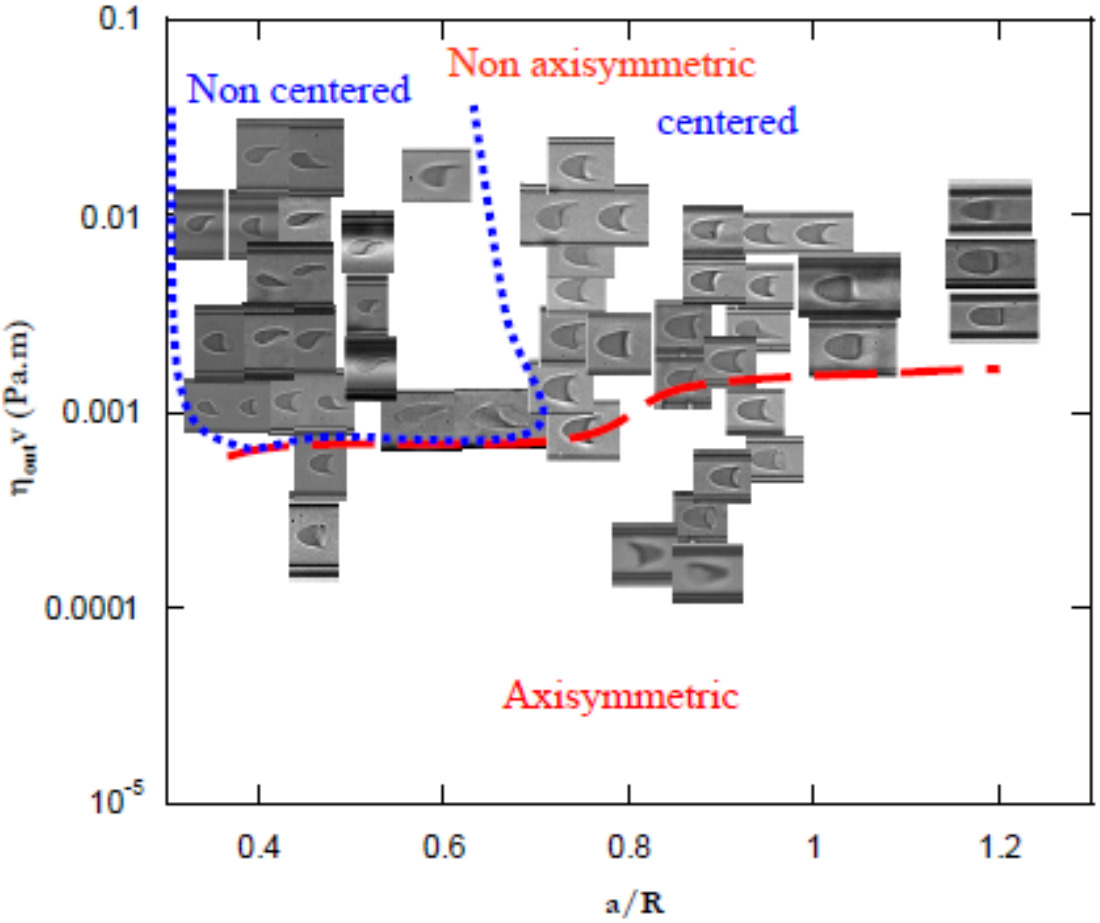


***Figure 3.5: The phase-diagram of the shape of RBCs (source: Faivre [18])***

In the model developed in this MSc thesis, the radius of the microtube is about 40 times diameters of the RBC. Moreover, the axial velocity of RBCs is set to be 1.505 cm/s. Therefore, indeed the value of the flow rate for the model here presented is satisfying the range of velocities of flow from 0.7 cm/s to 17 cm/s in the experiments by Faivre [18] (as it is shown in Figure 3.4). Therefore, the left top corner, where the radius *R* of the capillary is very small compared to typical size of the RBC and velocity of flow is about 1.505 cm/s, corresponds to the region of the interest of the present thesis.

The full transition from regular discocyte shape of the RBC to non-axisymmetric slipper-like shape happens in the range of external stress $\eta_{out}V$ from 0.001 to 0.01. Retrieving velocities:

$$\text{from } 0.001 \text{ to } 0.01 = \eta_{out}V \tag{3.1}$$

$$V = \frac{(\text{from } 0.001 \text{ to } 0.01)\ \text{Pa} \times \text{m}}{0.0012\ Pa \times s} = \text{from } 0.83 \text{ to } 8.3\ (m/s) \tag{3.2}$$

Corresponding the range of Reynolds numbers is:

$$Re = \frac{VD_{RBC}\rho_{plasma}}{\vartheta_{plasma}} \tag{3.3}$$

$$Re(V \text{ from } 0.83 \text{ to } 8.3\ (m/s)) = \frac{(\text{from } 0.83 \text{ to } 8.3) * 8 * 10^{-6} * 1{,}040}{0.0012} = \\ = 5.75 - 57.5$$

## 3.2 Establishing the relation between the shape of RBC and flow characteristics

The proposed present model is oriented to reproduce evolution of the shape of RBCs presented in the study by Faivre [18] throughout the range of Reynolds number, such that each shape, which can be observed in the phase diagram (Figure 3.5), corresponds to determined velocity of flow and the Reynolds number

accordingly. The five different shapes of the RBC, each of them corresponds to the determined Reynolds number, are modeled using ANSYS Design Modeler. In order to simulate volume preservation of RBCs, all the shapes have approximately the same volume with a maximum relative error of 0.1%. Table 3.1 shows evolution of five shapes of RBC, which are observed from the phase diagram (Figure 3.5), as the flow rate of blood increases.

***Table 3.1: Evolution of the RBC shape and its flow characteristics as the flow rate increases***

| # | **Shape** | $\eta_{out}V$ **(Pa×*m*)** | **Diameter of RBC (mm)** | **Velocity of flow (m/s)** | $c_d$ | ***Re*** |
|---|---|---|---|---|---|---|
| 1 |  | 0.0009-0.001 | 36 | 0.75-0.83 | 1.33 | 26.6-29.5 |
| 2 | 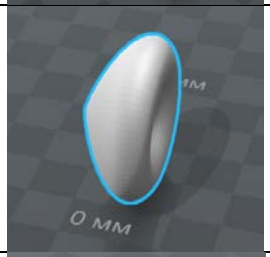 | 0.002 | 33.3 | 1.66 | 0.92 | 54.5 |
| 3 | 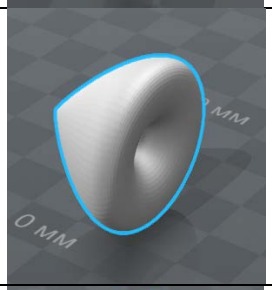 | 0.003 | 30.5 | 2.5 | 0.49 | 75.2 |
| 4 | 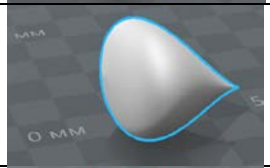 | 0.004 | 24.5 | 3.33 | 0.74 | 80.4 |
| 5 |  | 0.006 | 19.1 | 5 | 0.38 | 94.1 |

In order to obtain drag coefficient $c_d$ between the RBC and plasma in flow with dependence on local flow condition, experiments with a virtual wind tunnel were conducted.

The calculations of Reynolds numbers of each shaped cell, which is placed in a CFD virtual wind tunnel, are presented below:

$$Re\left(V = \frac{0.75m}{s}\right) = \frac{0.75 * 36 * 10^{-3} * 1.1839}{0.0012} = 26.6$$

$$Re\left(V = \frac{0.83m}{s}\right) = \frac{0{,}83 * 36 * 10^{-3} * 1.1839}{0.0012} = 29.5$$

$$Re\left(V = \frac{1.66m}{s}\right) = \frac{1.66 * 33.3 * 10^{-3} * 1.1839}{0.0012} = 54.5$$

$$Re\left(V = \frac{2.5m}{s}\right) = \frac{2.5 * 30.5 * 10^{-3} * 1.1839}{0.0012} = 75.2$$

$$Re\left(V = \frac{3.33m}{s}\right) = \frac{3.33 * 24.5 * 10^{-3} * 1.1839}{0.0012} = 80.4$$

$$Re\left(V = \frac{5m}{s}\right) = \frac{5 * 19.1 * 10^{-3} * 1.1839}{0.0012} = 94.1$$

The virtual tunnel model is validated by Flow Design software by Autodesk. Flow Design is similar to Autodesk CFD. Its meshing technology accepts geometries from wide range of CAD softwares. It runs transient incompressible flow solver using finite volume method [23]. Turbulence modeling is based on Smagorinsky Large Eddy simulations. Flow Design is available in some CAD software as a package, where it have can build wind tunnel around the model. Simulations with a wind tunnel, where a car were placed, using ANSYS FLUENT were conducted in order to compare results wind standalone

Flow Design software [23]. The model developed using Flow Design software demonstrated good approximation with CFD analysis using ANSYS FLUENT, where simulating a car in a wind tunnel requires, firstly, verification of wind tunnel itself, then CFD test on a car. It takes considerable time for model preparation and computational runtime. On the other hand, simulations using Flow Design software allows inexpensively and accurately evaluating design problems. Experiments in industrial facility were conducted as well in order to validate Flow Design software. Figure 3.11 demonstrates the results of the study. The virtual wind tunnel by Flow Design shows the relative error of 6% compared to the results of industrial experiments.

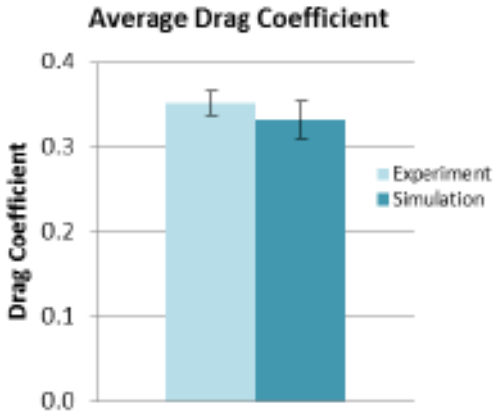


***Figure 3.11: Average drag coefficient comparison (image courtesy of [23])***

Each shape of the RBC is placed in the wind turbine in a manner that the gap between the walls of the wind turbine should be from two to three dimensions of the model with respect to all directions (see Figure 3.12-3.13). The dimensions, especially the length (see Figure 3.12) of the wind tunnel should allow correct

formation of the wake. Too small dimensions will let the air have been squeezed, that might result in wrong wake streams, faster air flow and higher drag forces [24].

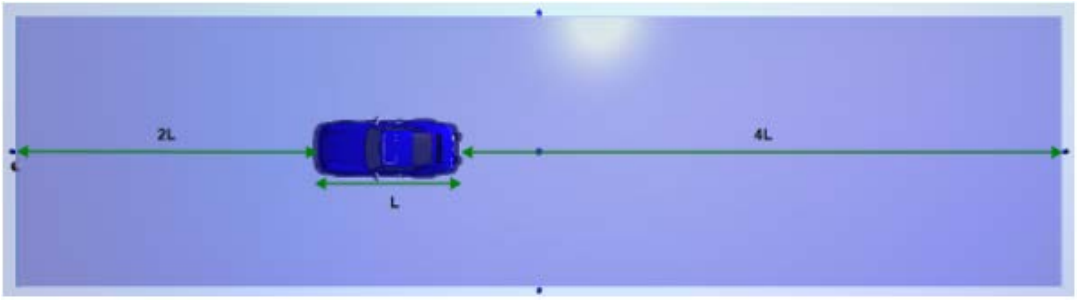


***Figure 3.12: Setting the length of the wind tunnel (image from Autodesk Flow Design Help)***

Figure 3.13 shows the guidelines on setting the width of the wind turbine.

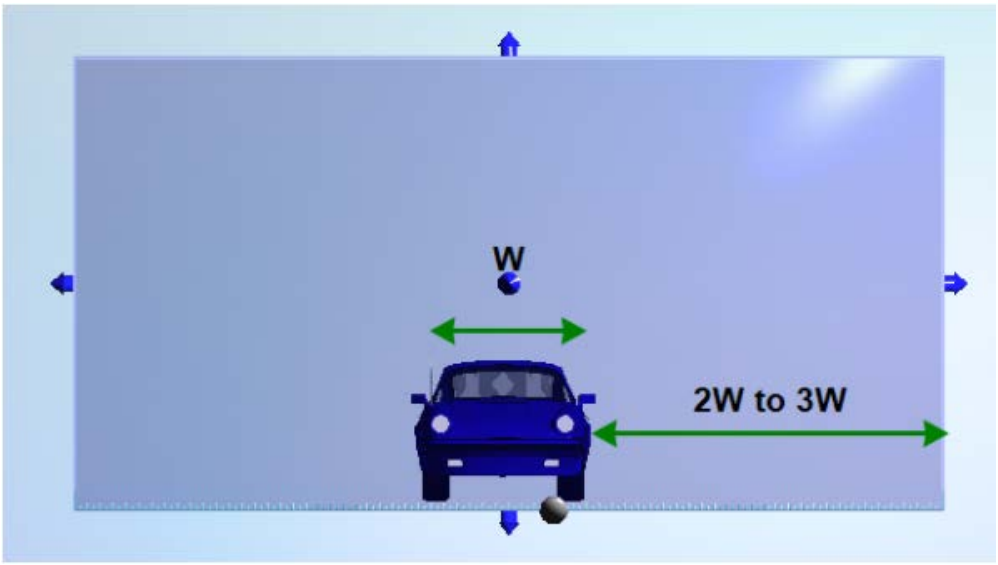


***Figure 3.13: Guidelines for setting the width of the wind tunnel (image from Autodesk Flow Design Help)***

Each shaped cell from Table 3.1 was placed against the wind with the velocity ranging from 0.75 m/s to 5 m/s. The CFD model led to value of drag

coefficient of each shaped cell accordingly. The velocity range was chosen in a manner that the calculated range of Reynold numbers comply with the range of Reynolds numbers in (3.3), which are obtained from the experiments with the flow of RBCs by Faivre [18]. Figure 3.6 shows the first non-deformed discocyte shape of the RBC placed in the virtual wind tunnel. The calculated drag coefficient is 1.33, which is the highest value among all shapes.

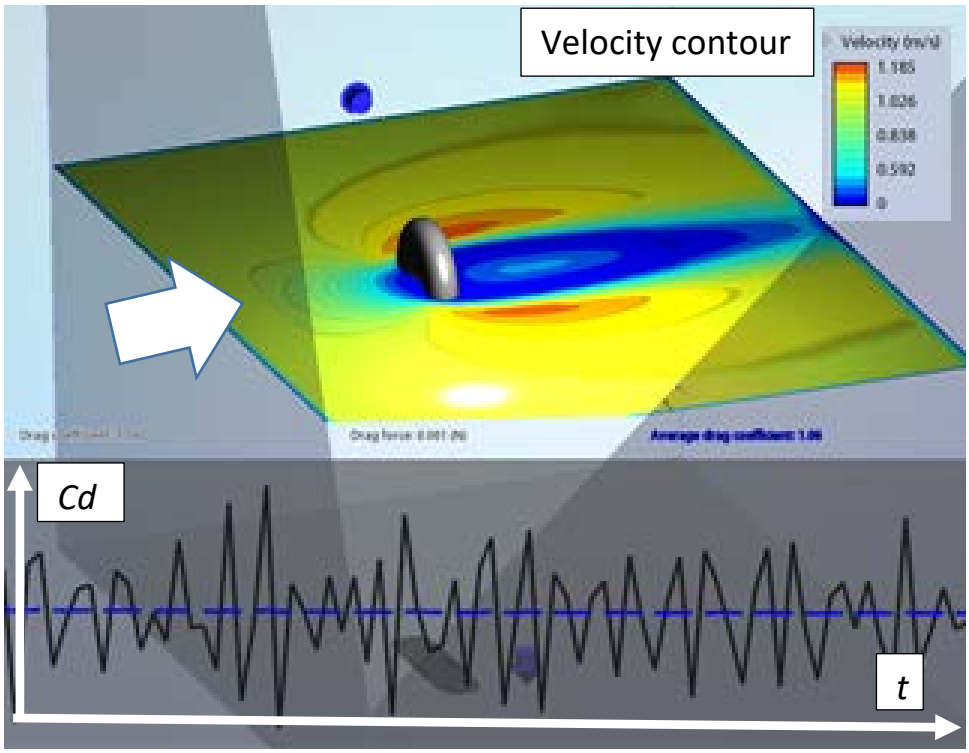


***Figure 3.6: Experiments with the first shape from Table 3.1 in the virtual wind tunnel***

Figure 3.7 represents the next shape of the RBC, which has been deformed and have a parachute-like form. The calculated drag coefficient for this shape is 0.92.

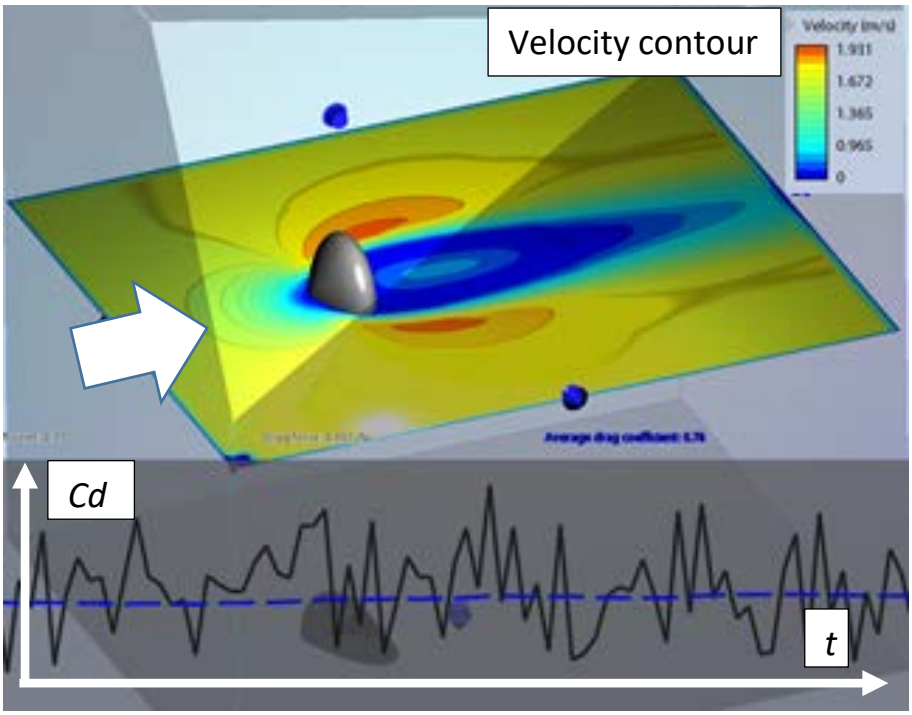


***Figure 3.7. Experiments with the second shape from Table 3.1 in the virtual wind tunnel***

Figure 3.8 demonstrates experiments with the parachute-like shape of the RBC, which is more bended than the previous shape. The yellow coloured plane represents the velocity profile inside the wind turbine. The drag coefficient is 0.49.

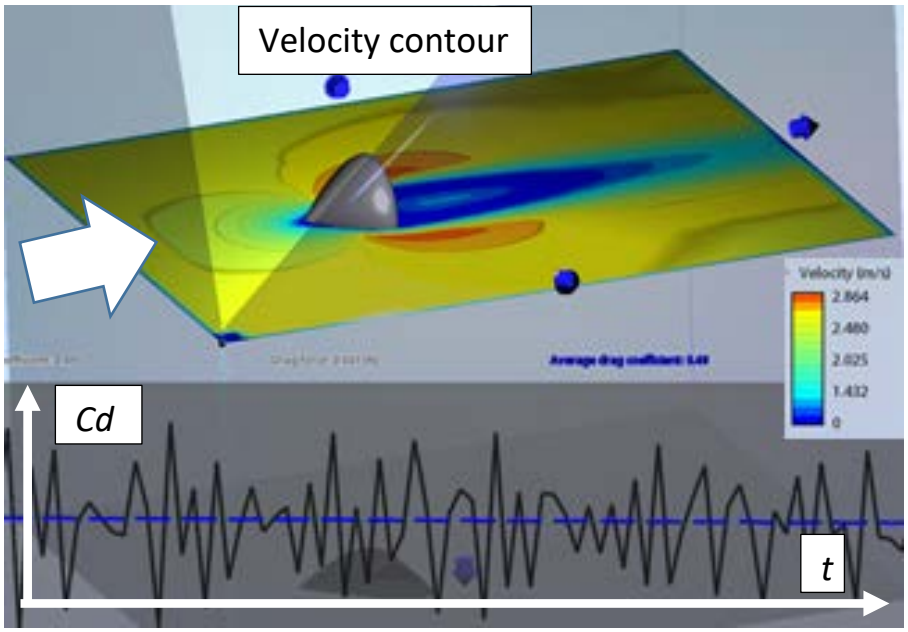


***Figure 3.8: Experiments with the third shape from Table 3.1 in the virtual wind tunnel***

As it can been from Figure 3.9, the form of the RBC turned to slipper-like shape. The calculated drag coefficient is 0.74.

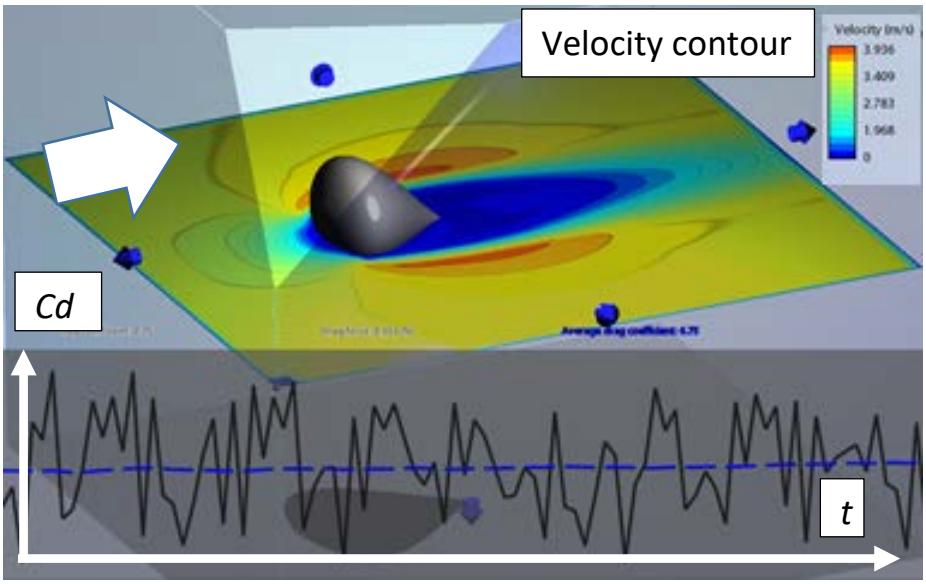


***Figure 3.9: Experiments with the fourth shape from Table 3.1 in the virtual wind tunnel***

The experiment with the last shape of the RBC is presented below in Figure 3.10. The shape also has non-symmetrical and slipper-like shape, however, deformed to a greater extent than the previous shape.

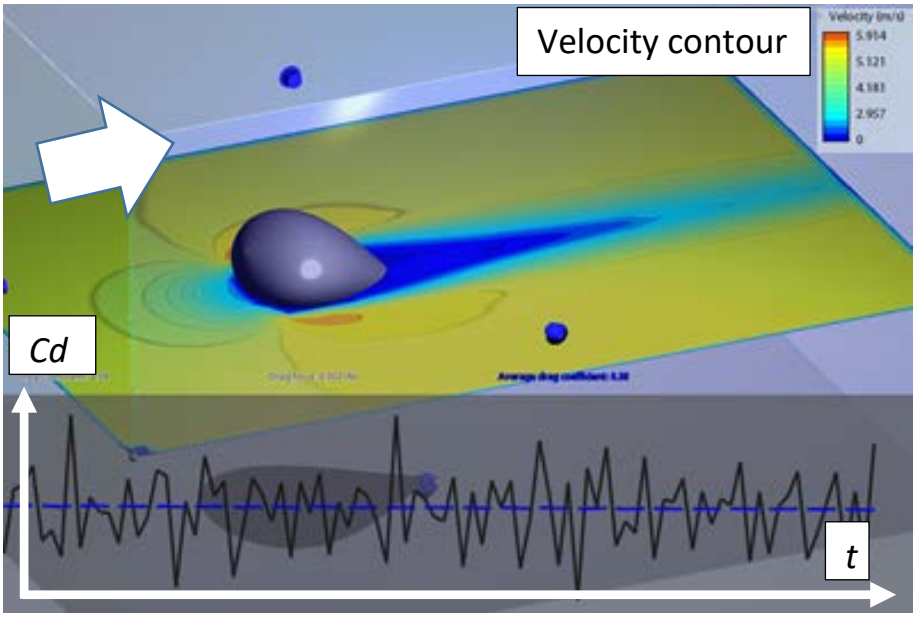


***Figure 3.10 Experiments with the fifth shape from Table 3.1 in the virtual wind tunnel***

As the result of experiments with the virtual wind tunnel, flow properties such as Reynolds number and drag coefficient for each RBC shape are obtained. As it was stated before, the Reynolds numbers from the virtual wind tunnel are similar to those used in the study by Faivre [18]. The range of drag coefficients from 0.38 to 1.33 agrees with typical drag coefficients in model by Mendygarin [4]. However, one important point should be noted regarding the Reynolds numbers from the work by Faivre [18]. Even though in experiments by Faivre [18] RBCs were moving within the flow in the tube, it is assumed the existence of relative motion between plasma and RBCs. Since RBCs deform under the pressure of the flow, which proves that there is drag between the RBC and plasma Nonetheless, here it is assumed the non-slip velocity between plasma and RBCs and consider the Reynolds number of the RBC the same as for the flow.

In order to incorporate shape deformation of RBCs into the CFD model, the drag coefficient as a function of Reynolds number is introduced by using data from the Table 3.1 and Curve Fitting tool of MATLAB. The data is fitted by regression using polynomial function with degree of 2. The function is as follows:

$$c_d = 0.00005847Re^2 - 0.02132Re + 1.904 \tag{3.4}$$

The coefficients of the function are with 95% confidence bounds. SSE (sum of squared errors) is 0.0512, R-square is 0.9099 and RMSE (root-mean-square deviation) is 0.1599.

# Chapter 4 – Implementation

## 4.1 Implementation of user-defined function

A uniform velocity profile is prescribed for the blood flow at the entrance in the proposed model. The inlet flow for all phases to be $1.505\times10^{-2}$ m/s in order to have all axial velocities equivalent to the Poisseuille wall shear rate 555 $s^{-1}$ used by Yeh et al. [6]. The radial velocities are set to be zero. Later, velocity develops a parabolic profile, represented in Figure 4.1. The gravitational force is set perpendicular to the tube length axis, where the Froude number is equal to 0.33.

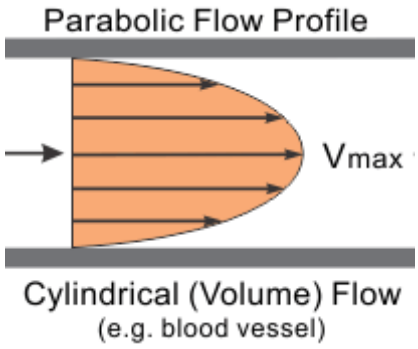


***Figure 4.1: Flow rate-driven flow (source: http://www.cvphysiology.com/Hemodynamics/H006)***

The average velocity through the microtube is equal to:

$$\vec{U}_{average} = \frac{\forall}{Area} \tag{4.1}$$

The overall Reynolds number in the tube is equal to:

$$Re_{overall} = \frac{\vec{U}_{average} D_{tube}}{\vartheta_{blood}} \tag{4.2}$$

One of the important points that the proposed model calculates local Reynolds number of RBCs in every point of the domain:

$$Re_{RBC} = \frac{U_{load} D_{RBC}}{\vartheta_{plasma}} \tag{4.3}$$

where $U_{load}$ is the velocity of the RBC at the determined point of the domain:

$$U_{load}(u_x, u_y, u_z) = \sqrt{u_x^2 + u_y^2 + u_z^2} \tag{4.4}$$

In order to incorporate the model developed in previous chapter that takes into account the shape evolution of the RBC across the flow with dependence on local flow conditions, drag coefficient between the RBC and plasma as a function of local Reynold number of the RBC is introduced. The function is developed as a user-defined function (UDF) for implementation of the developed drag law in ANSYS FLUENT. The UDF is written in C language (attached in Appendix A) and uses predefined macros and functions to access the data of ANSYS FLUENT solver. Compiled UDF is built and loaded to ANSYS FLUENT solver. After that,

UDF is hooked to ANSYS FLUENT solver by clicking to ‘user-defined’ in dialog box and selecting the name of the UDF at the ‘Phase interaction->Drag’ tab.

## 4.2 Mathematical model

Basic equations of mass and momentum conservation for plasma, RBCs and PLTs are prescribed as follow:

Plasma mass balance:

$$\frac{\partial(\rho_f \varepsilon_\mathrm{f})}{\partial t} + \nabla \bullet \left(\rho_f \varepsilon_\mathrm{f} \overrightarrow{\mathrm{v_f}}\right) = 0 \tag{4.5}$$

RBCs mass balance:

$$\frac{\partial(\rho_r \varepsilon_\mathrm{r})}{\partial t} + \nabla \bullet (\rho_r \varepsilon_\mathrm{r} \overrightarrow{\mathrm{v_r}}) = 0 \tag{4.6}$$

PLTs mass balance:

$$\frac{\partial(\rho_s \varepsilon_\mathrm{s})}{\partial t} + \nabla \bullet (\rho_s \varepsilon_\mathrm{s} \overrightarrow{\mathrm{v_s}}) = 0 \tag{4.7}$$

where $\rho$ is density, $\vec{V}$ is velocity, $\varepsilon$ is the volume fraction of each phase, $t$ is time.

Plasma momentum balance:

$$\frac{\partial\left(\rho_f \varepsilon_\mathrm{f} \vec{\mathrm{v}}_\mathrm{f}\right)}{\partial t} + \nabla \bullet \left(\rho_f \varepsilon_\mathrm{f} \overrightarrow{\mathrm{v_f}} \vec{\mathrm{v}}_\mathrm{f}\right) = \rho_f \varepsilon_\mathrm{f} \vec{\mathrm{g}} - \varepsilon_\mathrm{f} \nabla P + \nabla \bullet \vec{\vec{\tau}}_f + \beta(\vec{\mathrm{v}}_\mathrm{s} + \overrightarrow{\mathrm{v_r}} - \vec{\mathrm{v}}_\mathrm{f}) \tag{4.8}$$

RBCs momentum balance:

$$\frac{\partial(\rho_r \varepsilon_r \vec{v}_r)}{\partial t} + \nabla \cdot (\rho_r \varepsilon_r \overrightarrow{v_r} \vec{v}_r) = \rho_r \varepsilon_r \vec{g} - \varepsilon_r \nabla P - \nabla P_r + \nabla \cdot \vec{\vec{\tau}}_r + \beta(\vec{v}_f + \overrightarrow{v_s} - \overrightarrow{v_r}) \quad (4.9)$$

PLTs momentum balance:

$$\frac{\partial(\rho_s \varepsilon_s \vec{v}_s)}{\partial t} + \nabla \cdot (\rho_s \varepsilon_s \overrightarrow{v_s} \vec{v}_s) = \rho_s \varepsilon_s \vec{g} - \varepsilon_s \nabla P - \nabla P_s + \nabla \cdot \vec{\vec{\tau}}_f + \beta(\vec{v}_f + \overrightarrow{v_r} - \overrightarrow{v_s}) \quad (4.10)$$

where $\vec{g}$ is a gravity, $P$ is a fluid pressure, $P_s$ is a granular pressure, $\beta$ is the interface momentum exchange coefficient and $\vec{\tau}_r$ is the stress tensor.

The sum of volume fractions has to be one:

$$\varepsilon_f + \varepsilon_r + \varepsilon_s = 1 \quad (4.11)$$

The random kinetic energy for RBCs:

$$\frac{3}{2}\left[\frac{\partial(\rho_r \varepsilon_r \theta)}{\partial t} + \nabla \cdot (\rho_r \varepsilon_r \theta \overrightarrow{v_r})\right] = \left(-P_r \vec{\vec{I}} + \vec{\vec{\tau}}_r\right) : \nabla \vec{v}_r + \nabla \cdot (k_r \nabla \theta) - \gamma \quad (4.12)$$

The random kinetic energy for PLTs:

$$\frac{3}{2}\left[\frac{\partial(\rho_s \varepsilon_s \theta)}{\partial t} + \nabla \cdot (\rho_s \varepsilon_s \theta \overrightarrow{v_s})\right] = \left(-P_s \vec{\vec{I}} + \vec{\vec{\tau}}_s\right) : \nabla \vec{v}_s + \nabla \cdot (k_s \nabla \theta) - \gamma \quad (4.13)$$

where $\theta$ is the granular temperature, $k$ is the granular conductivity, $\gamma$ is the collisional dissipation. The granular temperature, as it was mentioned previously,

is the driven force for the particles migration, measured by the kinetic energy per unit mass and produced due to viscous type dissipation.

### 4.3 Physical properties and numerical set-up

The proposed model considers blood as a multiphase substance composed of plasma, RBCs and PLTs. Simulations depart from an existing Eulerian-Eulerian multiphase model and GKT for treatment of disperse phases (RBCs and PLTs). The computational domain is represented by a narrow tube with the length of 100 mm and fixed cross section with internal diameter equal to 217 μm, which is equivalent to about 40 Sauter diameters of the RBC (see Figure 4.2). The computational tube is axis-symmetrical and chosen the same as in experiments by Yeh et al [6].

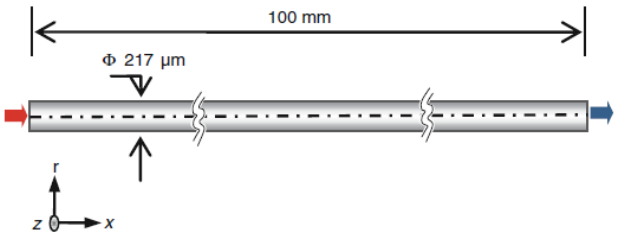


***Figure 4.2: Computational domain (source: Yeh et al. [6])***

During the computations, the inner part of the tube is filled by mixture of plasma, RBCs and PLTs with volume fractions of 58%, 40% and 2%, respectively. Plasma is modeled as a continuous Newtonian fluid. Viscosity of plasma is set to be 0.0012 Pa×s, density is 1,025 kg/m$^3$. RBCs and PLTs are modeled as sphere-like dispersed fluid. Viscosities of RBCs and PLTs are not

empirical parameter in this model, they are calculated by the GKT expressions. Density of the RBCs is set to be 1,100 kg/m$^3$. Density of the PLTs is set to be 1,040 kg/m$^3$. Sauter diameter of the PLT is 2.5 μm and 5.5 μm for RBC. Values for Sauter diameters are taken from the physical set-up of the model by Mendygarin et al. [4], as they represented the maximum improvement of peak PLTs concentration in previous work. Granular temperature for disperse phases is set to $10^{-8}$m$^2$/s$^2$. Parameters of the flow are summarized on the Table 4.1.

***Table 4.1: Flow parameters***

| **Phase** | **Plasma** | **RBC** | **PLT** |
|---|---|---|---|
| **Density** [kg/m$^3$] | 1,025 | 1,100 | 1,040 |
| **Viscosity** [kg/m×s] | 0.0012 | GKT | GKT |
| $D_p[\mu m]$ | - | 5.5 | 2.5 |
| **Volume Fraction** [%] | 58 | 40 | 2 |
| **Flow rate** [m/s] | $1.505\times10^{-2}$ | $1.505\times10^{-2}$ | $1.505\times10^{-2}$ |

No slip condition is assumed in the walls, outlet boundary is assumed to have no stress condition. The order of $10^{-8}$ is set for the accepted normalized errors, convergence of momentum, volume fraction and granular temperature equations. QUICK solution method is applied for the spatial discretization of the convective term. Simulations are performed in ANSYS FLUENT Academic version 18.2.

## 4.4 Verification of mesh independence

In order to ensure the independence of solution from mesh resolution, and find a numerical solution that is virtually independent of the mesh sizing, a study

of mesh convergence is conducted. Started from initial coarse grid, then gradually doing refinements, the effect of mesh on the results are observed. Three consecutive meshes with hexahedral elements (coarse, medium and fine) are developed using Fluent Mesh. Mesh carefully modeled near the edge regions by reducing the size of elements. Table 4.2 presents the number of cells for each type of mesh. The refinement factor from the coarse to the medium mesh is $r_{21} = \frac{h_{coarse}}{h_{medium}} = 1.4$, from the medium to the fine mesh is $r_{32} = \frac{h_{medium}}{h_{fine}} = 1.4$ as well. This method compares three mesh sizes, based on Richardson Extrapolation.

***Table 4.2: Three mesh types with number of cells***

| **Mesh** | **Nodes** |
|---|---|
| Coarse | 201810 |
| Medium | 309876 |
| Fine | 488250 |

Figure 4.3 shows relative PLTs concentration in a section far from the inlet of the microtube at the distance of 70 mm. Relative concentration of PLTs defined as a ratio of the concentration to the volume fraction:

$$Relative\ Conc = \frac{\varepsilon_{PLTs}}{\varepsilon_{prom.PLTs}}$$

Relative PLTs concentration using three different mesh types plotted in Figure 4.3. As it can be seen from Figure 4.3, refinement from the coarse mesh to the medium type produced small errors. However, the fine mesh unexpectedly

demonstrated lower peak value of PLTs than coarse and medium grids. Nevertheless, all meshes demonstrated similar relative PLTs concentration near the wall. As the result, medium mesh is selected for further study.

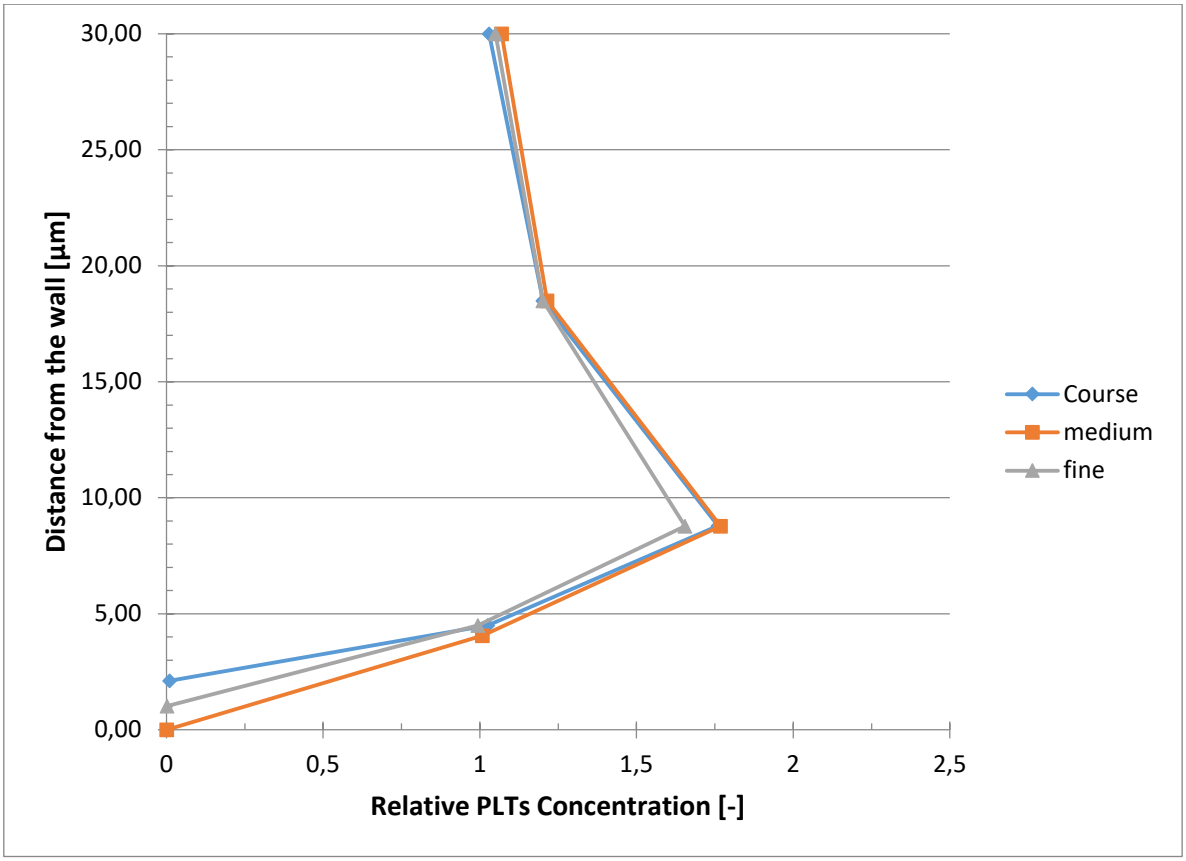


***Figure 4.3: Relative concentration of PLTs using three types of mesh***

## 4.5 Results and discussions

The relative difference in mass flow between inlet and outlet of the tube amounted to: for plasma $1.85\times10^{-3}$ %, for RBCs $2.58\times10^{-3}$ %, for PLTs $1.12\times10^{-3}$ % and $5.8\times10^{-3}$ % for all fluids, which demonstrates the convergence of simulations.

The section far from the inlet of the microtube at distance of 70 mm is selected for analysis.

Figure 4.4 represents volume fraction of RBCs in the prescribed section of the microtube. It can be seen, that RBCs tend to accumulate at the bottom part of the microtube. Since RBCs are denser than PLTs and plasma, the higher magnitude of gravitational force for RBCs prompts them to move toward the bottom of the microtube.

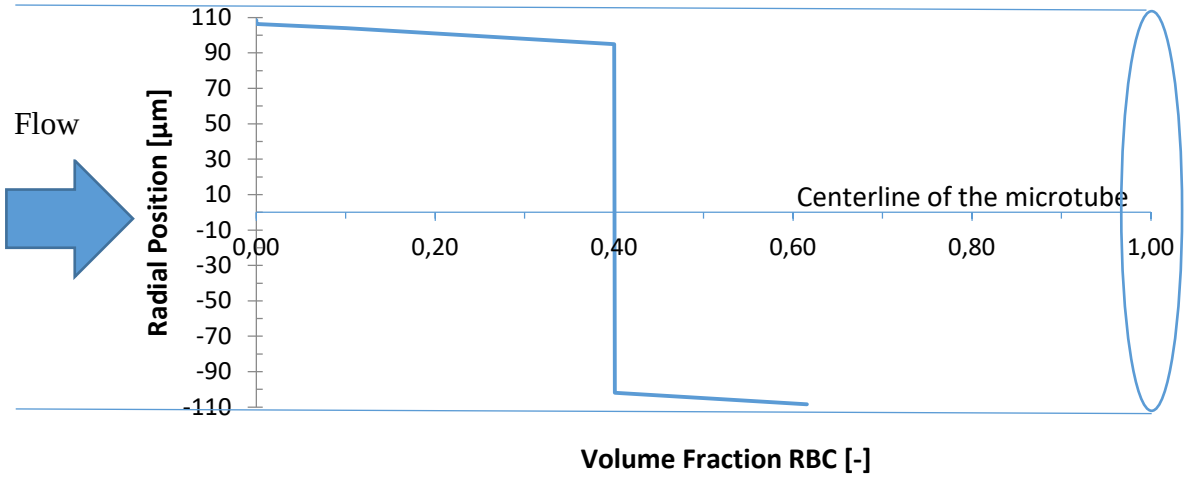


***Figure 4.4: Volume fraction of RBCs***

As the RBCs settled at the bottom, these cells force PLTs to move toward the upper part of the microtube. Therefore, PLTs have the maximum concentration on the upper part of the pipe (Figure 4.5). Plasma also has the maximum concentration at the upper part of the microtube, as it is shown in Figure 4.6. This is a typical behavior of blood flow in the vessel, which size is larger with respect to the size of blood cells.

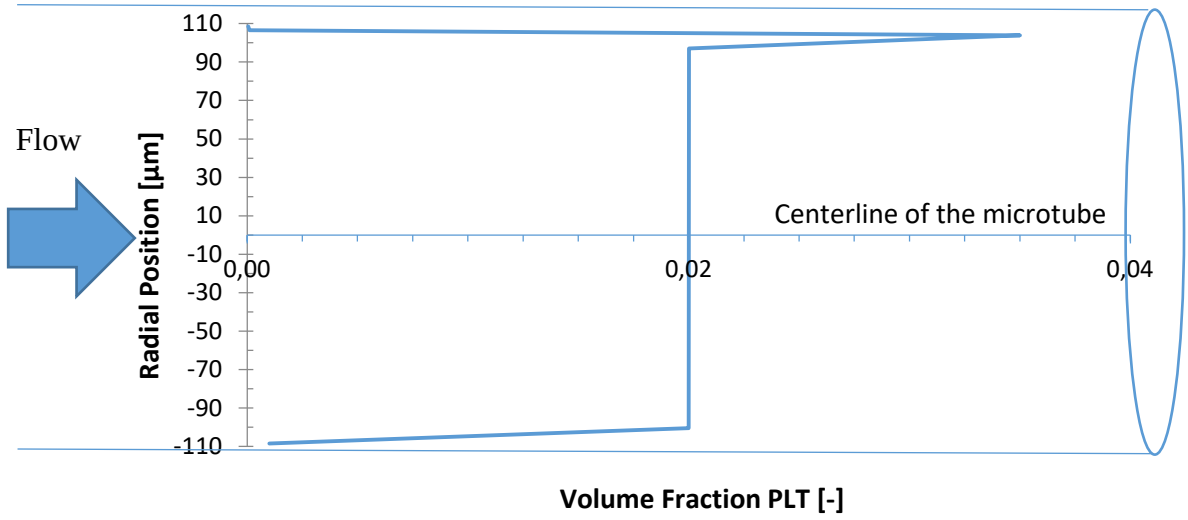


*Figure 4.5: Volume fraction of PLTs*

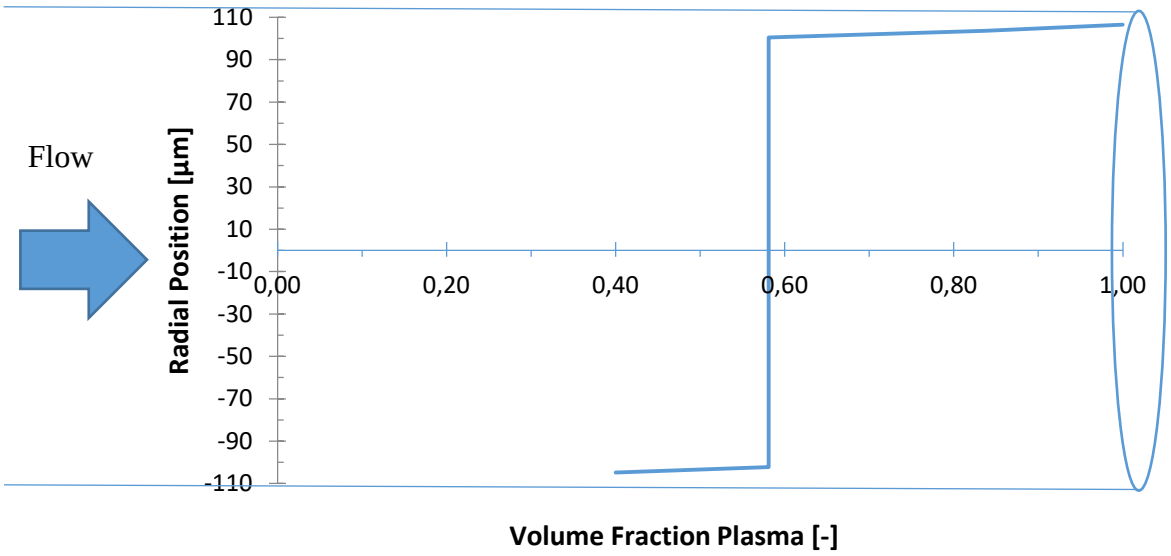


*Figure 4.6: Volume fraction of plasma*

The proposed model demonstrated relative PLTs concentration with the peak value at 1.77, which is lower than previous value found in model by Mendygarin et al. [4]. Both multiphase models' results approximately 6 times lower than experimental data by Yeh et al. [6]. PLTs tend to segregate at the distance near

the wall, which is known as the equilibrium position $y_e$ and is defined as the distance between the peak PLT concentration and the centerline of the microtube (r/R) [7]. The present model claims $y_e$ equal to 0.92, with the relative errors of 4% comparing to Mendygarin et al. and 6% comparing to experiments by Yeh et al. Relative PLTs concentrations of different models are plotted in Figure 4.7 and summarized on the Table 4.3.

***Table 4.3: Relative PLTs concentration by different models***

| **Model** | **Experimental data Yeh et al. [6]** | **Multiphase model Mendygarin et al. [4]** | **Multiphase model Supiyev** |
|---|---|---|---|
| **The peak of relative PLTs concentration** | 12 | 1.937 | 1.77 |
| **Equilibrium position $y_e$** | 0.98 | 0.96 | 0.92 |

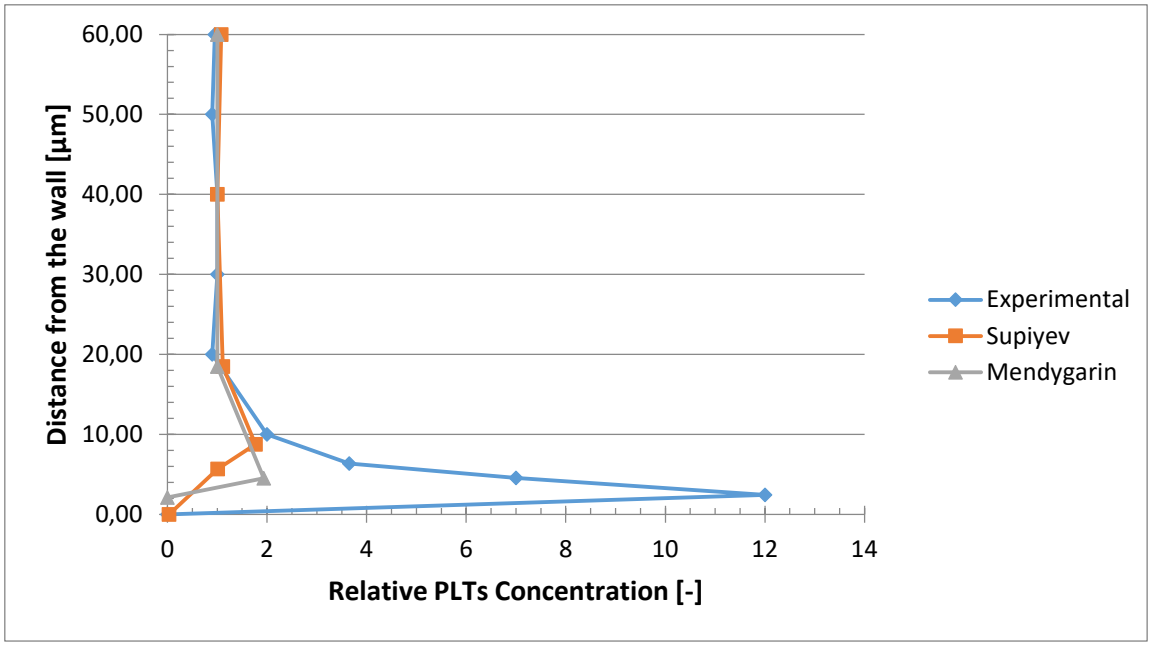


***Figure 4.7: Relative PLTs concentration by different models***

# Chapter 5 – Concluding remarks

This MSc thesis presents the results of an attempt to develop and validate through Fahraeus-Lindquist effect and experimental data by Yeh et al. [6] an improved model for blood cells segregation in flow through microtube. Previous model by Mendygarin et al. considers the RBC as a rigid sphere particle-like and their authors recognized that it is a very rough approximation [4]. This study hypothesized that incorporation of the RBC shape irregularities to the model will result in more realistic blood cells segregation in microtube. Therefore, the key point of this study was to take into account the shape deformation of RBCs with dependence on local flow conditions. Nonetheless, the proposed model did not show improvement of blood cells segregation. Moreover, simulations of the model show lower peak of PLTs relative concentration than previous model by Mendygarin et al. [4]. However, both multiphase models under-predict the peak concentration of PLTs near the wall, even though generally catch the segregation pattern. To conclude this study, the author believes that shape deformation and dynamics of RBCs should be taken into account in future work as it will help to develop realistic model of blood cells segregation in flow. The next step might be to improve existing model of the RBC shape evolution and consider realistic drag interaction between plasma and PLTs. The ulterior objective of course, would be to develop and validate blood damage model by incorporation of an improved

blood cells segregation model for further optimization of blood-wetted medical devices.

# Bibliography


[1] "Cardiovascular diseases (CVD)," World Health Organization, Retrieved from: http://www.who.int/mediacentre/factsheets/fs317/en/

[2] Salazar, A. Félix, Luis R. Rojas-Solórzano, and Armando J. Blanco, 2008, "Turbulence modeling in the numerical estimation of hemolysis in hemodialysis cannulae," Revista de la Facultad de Ingenieria UCV 23.4: 93-98

[3] "Computational Fluid Dynamics: An FDA Critical Path Initiative," Retrieved from: https://nciphub.org/wiki/FDA_CFD

[4] Mendygarin Y., Kussaiyn N., Luis R. Rojas-Solórzano, Zhussupbekov M., Supiyev R., 2017, "Eulerian-Eulerian Multiphase Modeling of Blood Cells Segregation in Flow through Microtubes," ASME IMECE 2017 Proceedings, in press

[5] Almomani T., Udaykumar H., Marshall J., Chandran K., 2008, "Micro-scale dynamic simulation of erythrocyte-platelet interaction in blood flow," Ann. Biomed. Eng. 36(6):905-920.

[6] Yeh, Chinjung, Anne C. Calvez, and Eugene C. Eckstein, 1994, "An estimated shape function for drift in a platelet-transport model," Biophysical journal 67.3: 1252-1259

[7] Mubita T. M., L. R. Rojas-Solórzano, and J. B. Moreno, 2014, "A Multiphase Approach to Model Blood Flow in Micro-tubes," Computational and Experimental Fluid Mechanics with Applications to Physics, Engineering and the Environment, Springer International Publishing: 235-247

[8] Gidaspow, Dimitri, and Jing Huang, 2009, "Kinetic theory based model for blood flow and its viscosity," Annals of biomedical engineering 37.8: 1534-1545

[9] Tandon, Elias, and Lo, 2015, "Comparative analysis of two multiphase modelling approaches for blood flow," Eleventh International Conference on CFD in the Minerals and Process Industries, CSIRO, Melbourne, Australia

[10] J. Sigüenza, 2016, "Fluid-structure interaction problems involving deformable membranes: application to blood flows at macroscopic and microscopic scales," Biomechanics [physics.med-ph], Université de Montpellier, <hal-01487308>

[11] E. A. Evans, and Y. C. Fung, 1972, "Improved measurements of the erythrocyte geometry," Microv. Res. 4:335–347

[12] N. Mohandas, and E. A. Evans, 1994, "Mechanical properties of the red cell membrane in relation to molecular structure and genetic defects," Ann. Rev. Biophys. Biomol. Struct. 23:787–818

[13] J. P. Mills, L. Qie, M. Dao, C. T. Lim, and S. Suresh, 2004, "Nonlinear elastic and viscoelastic deformation of the human red blood cell with optical tweezers," Mech. Chem. Biosys. 1(3):169–180

[14] M. Dao, C. T. Lim, and S. Suresh, 2003, "Mechanics of the human red blood cell deformed by optical tweezers," Journal of the Mechanics and Physics of Solids 51: 2259 – 2280

[15] Evans, E.A., Skalak, R., 1980, "Mechanics and Thermal Dynamics of Biomembranes," CRC Press, Boca Raton, FL

[16] Fung, Y.C. Biomechanics: Mechanical Properties of Living Tissues, 2nd Edition. Springer, New York, 1993

[17] T.W. Secomb. Modeling and Simulation of Capsules and Biological Cells. Chapman & Hall, London, 2003

[18] M. Faivre, 2006, "Drops, vesicles and red blood cells: Deformability and behavior under flow," Biological Physics [physics.bio-ph], Université Joseph-Fourier - Grenoble I, Retrieved from: https://tel.archives-ouvertes.fr/tel-00126365

[19] N. Takeishi, and Y. Imai, 2017, "Capture of microparticles by bolus flow of red blood cells in capillaries," Retrieved from: https://www.nature.com/articles/s41598-017-05924-7

[20] R. Skalak and P. I. Branemark, 1969, "Deformation of red blood cells in capillaries. Science," 164:717–719

[21] Y. Suzuki, N. Tateishi, M. Soutani, and N. Maeda, 1996, "Deformation of erythrocytes in microvessels and glass capillaries: effects of erythrocyte deformability," Microcirculation, 3:49–57

[22] C. Pozrikidis, 2005, "Axisymmetric motion of a file of red blood cells through capillaries," Physics of Fluids, 17:031503:1–14

[23] "Flow Design Preliminary Validation Brief," 2014, Retrieved from: http://download.autodesk.com/us/flow_design/Flow_Design_Preliminary_Validation_Brief_01072014.pdf

[24] "Flow Design Wind Tunnel," Retrieved from: https://knowledge.autodesk.com/support/flow-design/learn-explore/caas/CloudHelp/cloudhelp/ENU/FlowDesign/files/GUID-9B85F4A0-5072-454D-8710-CCFF26507BE9-htm.html

# Appendices

## Appendix A

The UDF for developed drag law between plasma and PLT

```
#include "udf.h"
#define pi 4.*atan(1.)


DEFINE_EXCHANGE_PROPERTY(new, cell, mix_thread, s_col, f_col)
{
	Thread *thread_p, *thread_rbc;
	real x_vel_p, x_vel_rbc, y_vel_p, y_vel_rbc, z_vel_p, z_vel_rbc, abs_v, slip_x,
slip_y, slip_z,
		rho_p, rho_rbc, mu_p, reyp, Res, afac, Cd,
		vof_p, vof_rbc, k_g_s, Ergun, WenYu, phi_gs, diam2, taup;

	/* find the threads for the plasma (primary) */
	/* and rbc (secondary phases) */

	thread_p = THREAD_SUB_THREAD(mix_thread, s_col);/* plasma phase */
	thread_rbc = THREAD_SUB_THREAD(mix_thread, f_col);/* rbc phase*/


	/* find phase velocities and properties*/

	x_vel_p = C_U(cell, thread_p);
	y_vel_p = C_V(cell, thread_p);
	z_vel_p = C_W(cell, thread_p);
	x_vel_rbc = C_U(cell, thread_rbc);
	y_vel_rbc = C_V(cell, thread_rbc);
	z_vel_rbc = C_W(cell, thread_rbc);

	slip_x = x_vel_p - x_vel_rbc;
	slip_y = y_vel_p - y_vel_rbc;
	slip_z = z_vel_p - z_vel_rbc;

	rho_p = C_R(cell, thread_p);
	rho_rbc = C_R(cell, thread_rbc);

	mu_p = C_MU_L(cell, thread_p);

	diam2 = C_PHASE_DIAMETER(cell, thread_rbc);

	/*compute slip*/
	abs_v = sqrt(slip_x*slip_x + slip_y*slip_y + slip_z*slip_z);

	/*compute Reynold's number*/

	reyp = rho_p*abs_v*diam2 / mu_p;

	/* compute volume fractions */

	vof_p = C_VOF(cell, thread_p);/* plasma vol frac*/
	vof_rbc = C_VOF(cell, thread_rbc);/* rbc vol frac*/

	/* compute particle relaxation time */
	taup = rho_rbc*diam2*diam2 / 18. / mu_p;
```

```
        if (reyp >= 1000)
               Cd = 0.44;
        else
               Cd = 5.847e-05*(pow(reyp, 2)) - 0.02132*reyp + 1.904;


        if (vof_p <= 0.8) {

               k_g_s = vof_rbc*rho_rbc*Cd / taup;

        }


        else
        {

               k_g_s = vof_rbc*rho_rbc*Cd / taup;
        }




        return k_g_s;
}
```